scientific reports

Check for updates

OPEN

Densification in transparent SiO_2 glasses prepared by spark plasma sintering

Hirokazu Masai[1]✉, Hiromi Kimura[2,8], Naoyuki Kitamura[1], Yuka Ikemoto[3], Shinji Kohara[4], Atsunobu Masuno[5], Yasuhiro Fujii[6], Takamichi Miyazaki[7] & Takayuki Yanagida[2]

Recently, spark plasma sintering (SPS) has become an attractive method for the preparation of solid-state ceramics. As SPS is a pressure-assisted low-temperature process, it is important to examine the effects of temperature and pressure on the structural properties of the prepared samples. In the present study, we examined the correlation between the preparation conditions and the physical and structural properties of SiO_2 glasses prepared by SPS. Compared with the conventional SiO_2 glass, the SPS-SiO_2 glasses exhibit a higher density and elastic modulus, but a lower-height first sharp diffraction peak of the X-ray total structure factor. Micro-Raman and micro-IR spectra suggest the formation of heterogeneous regions at the interface between the SiO_2 powders and graphite die. Considering the defect formation observed in optical absorption spectra, reduction reaction mainly affects the densification of SPS-SiO_2 glass. Hence, the reaction at the interface is important for tailoring the structure and physical properties of solid-state materials prepared by the SPS technique.

Ceramics have attracted attention from the viewpoint of functional materials with excellent thermal stabilities and chemical durabilities. Considering the Sustainable Development Goals (SDGs), the fabrication of functional materials is not only important scientifically but also environmentally. Because transparent ceramics are used for various optical applications, the available fabrication methods and materials have been investigated worldwide. The synthesis of conventional ceramics require energy, and an energy-less fabrication process is an important aspect of SDGs. One preparation method for obtaining transparent materials is spark plasma sintering (SPS)[1–10]. In contrast to conventional methods for ceramic synthesis, the SPS process enables sintering at a lower temperature and a shorter time by utilising electrical energy and the high energy of discharge plasma[1]. Although the size of the obtained solid is limited, sintering at a high pressure and low temperature is attractive for the preparation of novel functional materials, such as phosphors[7–10].

It has been reported that the properties of solid materials obtained by SPS are different from those of conventional materials or materials obtained by conventional sintering. Because the SPS technique has been developed for fabrication of materials, functionality seems to be the top priority for researchers. Detailed studies of physical and structural properties are important not only for the analysis of materials but also for the improvement of the SPS technique. Nevertheless, microscopic structural analysis by spectroscopy is considered secondary to the examination of functionality.

SiO_2 glass has been used as a fundamental optical material with high durability and chemical stability in optical fibres and substrates. Because of the high temperature involved in the fabrication, several attempts have been made to fabricate SiO_2 glass at low temperatures; these include liquid-phase methods (such as sol–gel) and SPS. SiO_2 glass prepared by SPS was first reported in the 1990s. The luminescence of SiO_2 glass containing activators prepared by sintering has been also reported[7–10]. Because SiO_2 glasses prepared by different methods exhibit different properties for different purposes and applications, it is very important to investigate the relationship

[1]Department of Materials and Chemistry, National Institute of Advanced Industrial Science and Technology, 1-8-31 Midorigaoka, Ikeda, Osaka 563-8577, Japan. [2]Graduate School of Materials Science, Nara Institute of Science and Technology, 8916-5, Takayama-cho, Ikoma, Nara 630-0192, Japan. [3]Japan Synchrotron Radiation Research Institute (JASRI/SPring-8), 1-1-1, Kouto, Sayo-cho, Sayo-gun, Hyogo 679-5198, Japan. [4]Research Center for Advanced Measurement and Characterization, National Institute for Materials Science, 1-2-1, Sengen, Tsukuba, Ibaraki 305-0047, Japan. [5]Graduate School of Science and Technology, Hirosaki University, 3 Bunkyo-cho, Hirosaki, Aomori 036–8561, Japan. [6]Department of Physical Sciences, Ritsumeikan University, 1-1-1 Noji-higashi, Kusatsu, Shiga 525-8577, Japan. [7]Technical Division, Graduate School of Engineering, Tohoku University, 6-6-11, Aoba, Sendai 980-8579, Japan. [8]National Institute of Advanced Industrial Science and Technology, 1-1-1 Umezono, Tsukuba, Ibaraki 305-8568, Japan. ✉email: hirokazu.masai@aist.go.jp

ID	Density (g cm^{-3})	Longitudinal sound velocity V_L (km/s) (±0.01)	Transverse sound velocity V_T (km/s) (±0.01)	Shear Modulus G_0 (GPa) (±0.1)	Poisson Ratio ν (±0.001)	Young Modulus E_0 (GPa) (±0.1)	Bulk Modulus K_0 (GPa) (±0.1)
Conventional SiO_2 glass	2.196 (±0.001)	5.96	3.79	31.6	0.160	73.3	35.9
1300 °C 70 MPa	2.221 (±0.001)	6.04	3.80	32.0	0.171	75.0	38.0
1300 °C 6 MPa	2.220 (±0.001)	6.03	3.81	32.2	0.168	75.1	37.7
1400 °C 70 MPa	2.224 (±0.001)	6.04	3.82	32.3	0.167	75.5	37.8
1400 °C 6 MPa	2.249 (±0.006)	6.12	3.84	33.1	0.176	77.8	40.0

Table 1. Physical properties of the SPS-SiO_2 glasses compared with those of conventional glass.

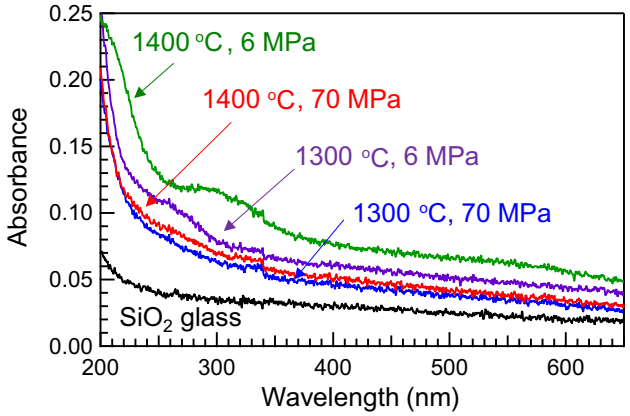

Figure 1. Optical absorption spectra of SPS-SiO_2 glasses prepared at different conditions along with that of SiO_2 glass.

between the structure and the physical properties of the prepared SiO_2 glass. However, a detailed study of the structure of SPS-SiO_2 glass is lacking. In this study, we performed a structural analysis of SiO_2 glass prepared by the SPS method and compared its characteristics with those of conventional SiO_2 glass. In addition, space-selective microscopic analysis was used to determine the spatial heterogeneity of SPS-SiO_2 glass.

Results and discussion

Optical and physical properties. The obtained SPS-SiO_2 glasses were transparent to the naked eye. In the previous report, SiO_2 glasses were prepared in the temperature range of 727–1427 °C at 100 MPa pressure, but transparent bulk material was obtained with the sintering temperature above 1250 °C[6]. Since transparent SPS-SiO_2 glass is the target of the study, four preparation conditions were used: 6 MPa, 1300 °C; 6 MPa, 1400 °C; 70 MPa, 1300 °C; and 70 MPa, 1400 °C. The physical properties of the prepared glasses are listed in Table 1. All the SPS-SiO_2 glasses exhibit higher densities than that of conventional SiO_2 glass. In addition, the dense SPS-SiO_2 glasses possess a higher G_0, E_0, and K_0 than those of conventional SiO_2 glass. Despite the same preparation conditions, the densities of the SPS-SiO_2 glasses were changed depending on the weight of starting chemicals. The lighter the starting material, the heavier the density. Notably, the dependence of the preparation conditions (temperature and pressure) on the elastic properties is obscure. Therefore, it is expected that not only the temperature, pressure, and heating program but also the volume of the starting material affects the nature of the obtained samples. Considering the mechanism of the SPS method, the distance between the graphite punches might affect the sintering efficiency and the resulting properties[14–16].

Figure 1 shows the optical absorption spectra of the glasses along with that of conventional SiO_2 glass. Small absorption bands are observed below 350 nm, which originate from the generation of defects, such as oxygen deficiency centres and dangling oxygen bonds[11–13]. It is notable that absorbance of the samples prepared at 6 MPa is higher than that of ones prepared at 70 MPa under the same preparation temperature. We also found that the increasing absorbance, i.e. defect formation, is suppressed by applying lower temperature under the same preparation pressure.

Positron annihilation spectroscopy (PAS) analysis. For structural analysis of the SPS-SiO_2 glasses, we performed PAS, which is used to quantify the cavity size in materials[17–20]. Figure 2 shows the positron decay curves of the SPS-SiO_2 and conventional SiO_2 glasses; there is no significant difference in the curves. For insulators, the decay constant of *ortho*-positronium (the third component in fitting the decay curve) is used for size calculation. The cavity radius of the SPS-SiO_2 glass was calculated to be 0.245 (±0.002) nm, which is almost identical to that of standard SiO_2 glass (0.247 nm) (Supplementary Table 1). This result is in accordance with

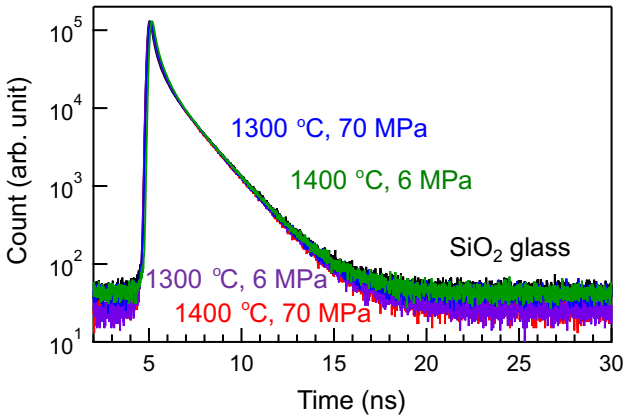

Figure 2. Positron decay curves of SPS-SiO_2 glasses prepared at different conditions along with that of conventional SiO_2 glass.

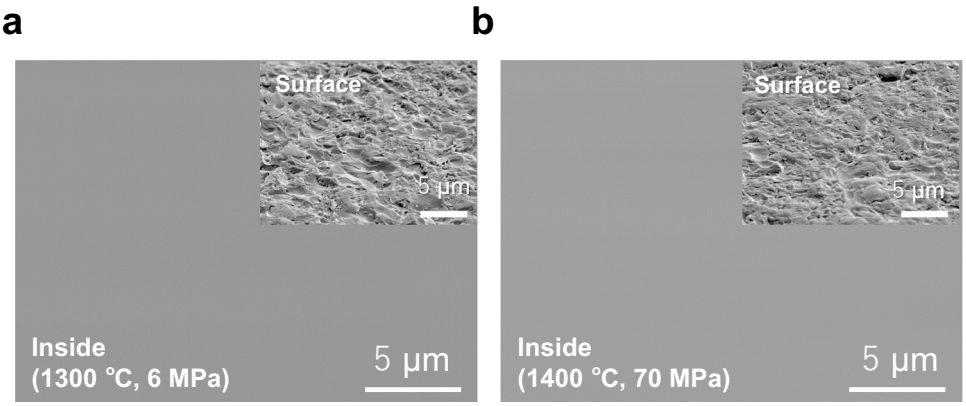

Figure 3. SEM observation of SPS-SiO_2 glasses. SEM images of interiors of the SPS-SiO_2 glasses prepared at 6 MPa, 1300 °C (**a**) and 70 MPa, 1400 °C (**b**), respectively. The insets show the surface of the samples. The surface and the interior of the samples were polished mechanically and by ion-milling, respectively.

the values published in the literature for densified silica glasses[20]. As reported previously[19], PAS tends to detect larger cavities (rather than smaller ones) in SiO_2 glass. Hence, the small changes observed in the density cannot be explained using the cavity sizes obtained by PAS as it is based on preferential annihilation of positrons in cavities. A microscopic analysis is expected to provide additional information to explain the densification of SPS-SiO_2 glasses.

Microscope observation. We performed Scanning Electron Microscope (SEM) and Transmission Electron Microscope (TEM) imaging of the surface and the interior to analyse the morphologies of the SPS-SiO_2 glasses.

Figure 3 shows the SEM images of SPS-SiO_2 glasses prepared at different conditions. Inset shows the surface of the samples by mechanically polishing. Inside the samples prepared by ion-milling, there are no grain boundaries originating from the SiO_2 powder, resulting in a uniform morphology. The fully sintered images at 1300 and 1400 °C are very similar to those in the previous paper[6]. It is natural that the obtained SPS-SiO_2 glasses without grain boundary exhibit the transparency over a wide wavelength range.

Figure 4 shows the TEM images of SPS-SiO_2 glasses prepared at different conditions. Both the surface and the interior of the samples are homogenous with no precipitation of crystallites. Hence, all the SPS-SiO_2 glasses are expected to be amorphous, which was confirmed by conventional XRD (discussed later). Because there is no clear evidence of densification in the TEM results, other analytical approaches are required.

High energy XRD (HEXRD) analysis. Based on the relationship between the first sharp diffraction peak (FSDP) of the X-ray total structure factor $S(Q)$ and the density of SiO_2 glasses (as reported in our recent study)[16], we focused on the FSDP profile of the SPS-SiO_2 glasses. The FSDP height at $Q = 1.55$ Å^{-1} strongly correlates with the structural disordering of glasses[21–25]. Figure 5a shows the $S(Q)$ of the SPS-SiO_2 glasses prepared at 70 MPa, 1400 °C along with that of SiO_2 glass. The X-rays were irradiated at the centre of the samples. The spectral shapes

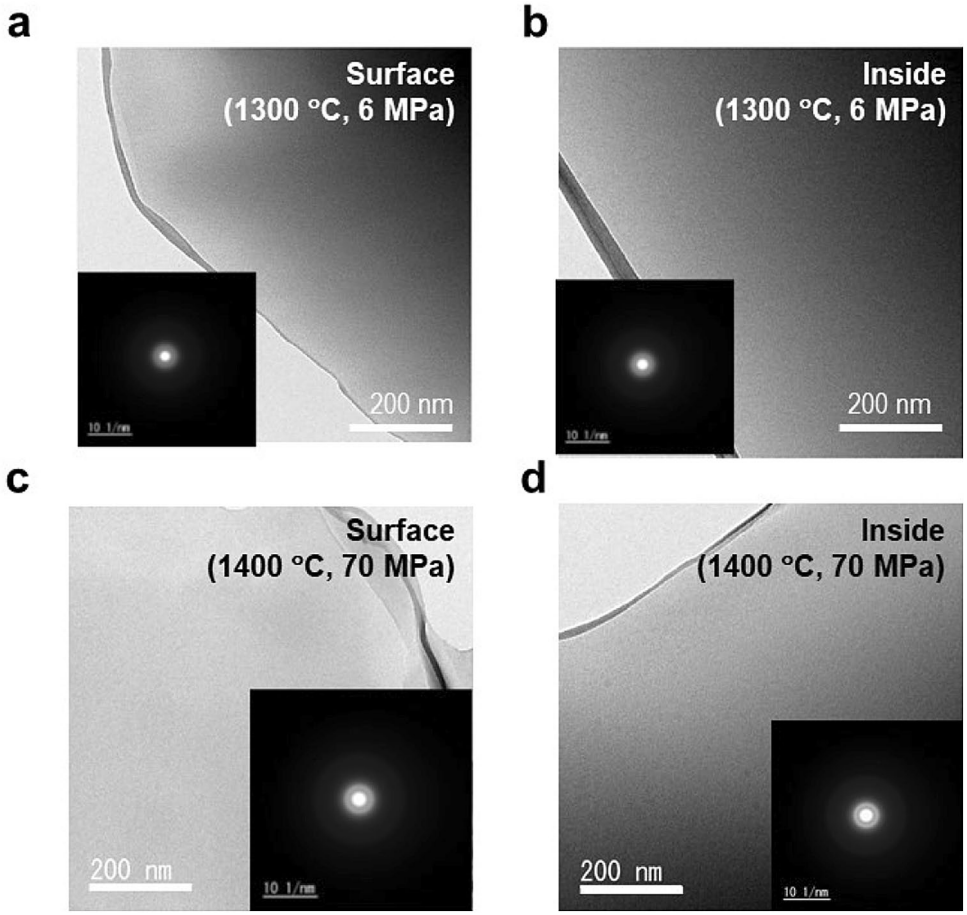

Figure 4. TEM observation of SPS-SiO_2 glasses. TEM images of the (**a**, **c**) surfaces and (**b**, **d**) insides of the SPS-SiO_2 glasses prepared at 6 MPa, 1300 °C and 70 MPa, 1400 °C, respectively.

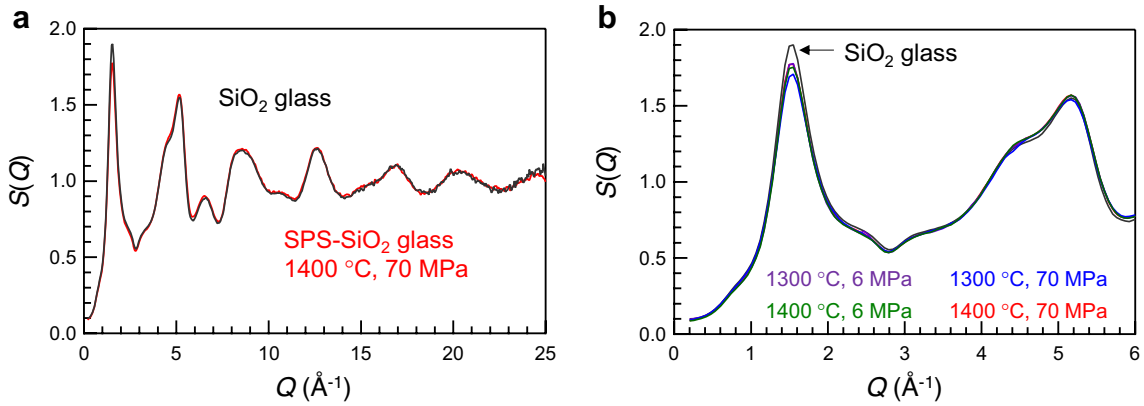

Figure 5. Comparison of $S(Q)$ of SPS-SiO_2 glass and SiO_2 glass. (**a**) $S(Q)$ of SPS-SiO_2 glass prepared at 70 MPa, 1400 °C along with that of SiO_2 glass. (**b**) Enlarged $S(Q)$ of SPS-SiO_2 glasses prepared at different conditions along with that of SiO_2 glass.

of both the samples are similar, and no sharp diffraction peak attributable to crystalline SiO_2 is observed. Similar shapes in the low- to high-Q regions confirm that no cluster-like structure is formed in the SPS-SiO_2 glass. Figure 5b shows the enlarged $S(Q)$ values of these glasses in the low-Q regions. Notably, there is a slight difference in the height of the FSDP. However, the relationships between the FSDP height and the SPS conditions or the density of SPS-SiO_2 glasses are not completely understood. Although we can conclude that the small difference in the FSDP height originates from the denser packing of the SiO_4 network by the SPS method, the detailed structure is not clear from these results.

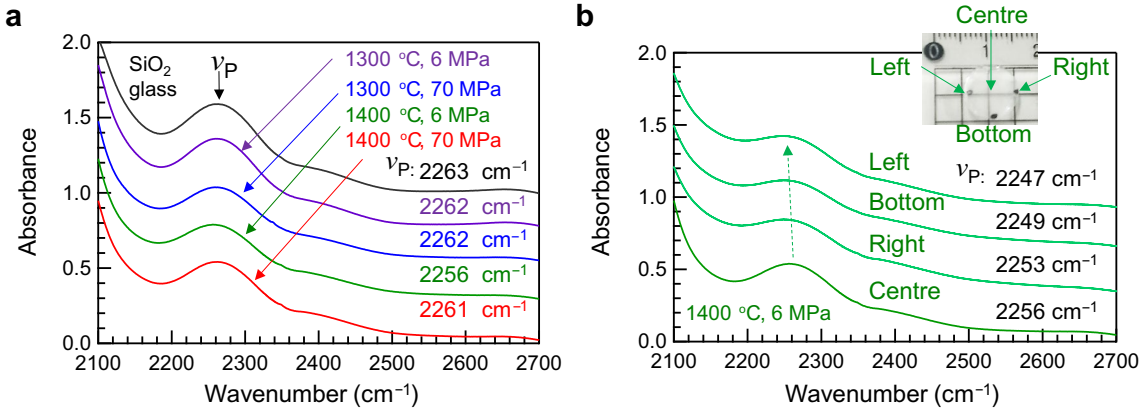

Figure 6. Spatial heterogeneity by micro-IR spectroscopy. (**a**) Micro-IR spectra of SPS-SiO_2 and SiO_2 glasses obtained from the centre. (**b**) Enlarged micro-IR spectra obtained from different positions of the SPS-SiO_2 glass prepared at 6 MPa, 1400 °C. The inset shows the photograph of the SPS-SiO_2 glass; the black dots at the edges indicate the measurement points.

IR and Raman spectroscopy. We used IR and Raman spectroscopy techniques to study the spatial heterogeneity of the SPS-SiO_2 glass. Figure 6a shows the micro-IR spectra of the SPS-SiO_2 glasses obtained from the centres of the SPS-SiO_2 and conventional SiO_2 glasses. Although the spectral shapes are similar, there is a slight shift in the band at approximately 2260 cm^{-1}. This vibration mode is an overtone of the Si–O–Si vibration mode, which is occasionally discussed from the viewpoint of fictive temperature (T_f) of SiO_2 glasses[15,16,26–33]. Notably, SPS-SiO_2 glass prepared at 6 MPa, 1400 °C, which exhibits the highest density among all the samples, exhibits the largest shift in the Si–O–Si peak. Figure 6b shows the enlarged microscopic IR spectra obtained from different positions of the SPS-SiO_2 glass prepared at 6 MPa, 1400 °C. The spectra obtained from the edges of the SPS-SiO_2 glass are different from that obtained from the centre of the sample; the Si–O–Si peak shifts to lower wavenumbers when moving from the left edge to the right. A shift to a lower wavenumber can be assigned to a higher T_f, i.e., not annealed. However, the peak shift in the present data is too large to explain this phenomenon from the viewpoint of merely the T_f of SiO_2 glass[16,29]. In addition, although the SPS-SiO_2 glasses were obtained by cooling without temperature control, the quenching rate was slower than the water-quenching rate of SiO_2 glass with a high T_f. Therefore, it is expected that this shift originates from the reaction at the interface between the SiO_2 powder and the surrounding graphite die.

In Raman spectroscopy, we focused on the boson peak and the vibrational modes at 490 cm^{-1} (D_1) and at 600 cm^{-1} (D_2)[34–39]. Therefore, we discuss Raman spectra measured with HH (parallel nicol) polarisation (Supplementary Fig. 1(a)). Although the origins of both these vibrational modes are not completely understood, the boson peak has been correlated with the free volume of glasses[40]. On the other hand, D_1 and D_2 are assigned to the vibration of four- and three-membered rings of SiO_4 tetrahedral units, respectively[39]. In contrast to conventional SiO_2 glass, SPS-SiO_2 glass exhibits fluorescence upon laser irradiation, suggesting the formation of defects in the matrix (Supplementary Fig. 1(b)). The expected defect generation is consistent with the results of optical absorption shown in Fig. 1. Considering the results of micro-IR spectroscopy, the Raman spectra were also obtained from three different points (shown in the inset of the photograph) on the samples. The broad baseline due to fluorescence was removed by applying an extended multiplicative signal correction (EMSC) algorithm, adopting the bulk SiO_2 glass spectrum without fluorescence as a reference. [41] Figure 7a shows the micro-Raman spectra of the SPS-SiO_2 (prepared at 6 MPa, 1400 °C) and conventional SiO_2 glasses; these spectra were recorded with HH polarisation. Although the spectral shapes are roughly similar, there is a slight difference between the spectra of SPS-SiO_2 and SiO_2 glasses. Figures 7b–d show the enlarged Raman spectra highlighting the boson, D_1, and D_2 peaks, respectively. The height of the boson peak of SPS-SiO_2 glass is comparable to that of the SiO_2 glass, and a remarkable peak shift is not observed. On the contrary, the intensities of the D_1 peak at 490 cm^{-1} (Fig. 7c) and the three-membered-ring (D_2) peak at 600 cm^{-1} (Fig. 7d) of SPS-SiO_2 glass increase. It is suggested that D_2 structures exist at the vicinity of SiO_2 surface[39]. Considering the result of PAS, in which a large cavity is not diminished by SPS, it is suggested that small silica units are formed at the edges of the sample (near the interface with the mould). Because the decrease in the height of FSDP in HEXRD (Fig. 5) also suggests a less ordered glass network, it can be concluded that a defect-like structure is generated in the SPS-SiO_2 glass. Notably, the height of the boson peak is comparable, although the shift in the Si–O–Si vibrational peak is the largest at the left edge of the sample (interface with the mould). The correlation between the Boson peak of silica glass and the average of distribution of Si–O–Si bonding angle is well established[42,43]. Since there is no visible correlation between the boson peak in the Raman spectrum and the Si–O–Si vibrational peak in the IR spectrum, it is expected that Raman spectroscopy is less sensitive to small density changes than IR spectroscopy.

The results of the present study suggest that the interface with the mould affects the properties of ceramics obtained by pressure-assisted fabrication under reduced atmosphere. We assume that the highest density of SPS-SiO_2 glass prepared at 6 MPa and 1400 °C is mainly due to reduction reactions, rather than conventional densification by applying pressure above several GPa. In addition, it is expected that higher pressure and lower temperature are effective to prevent reduction reaction. Even in the aerodynamic levitation method[44], where

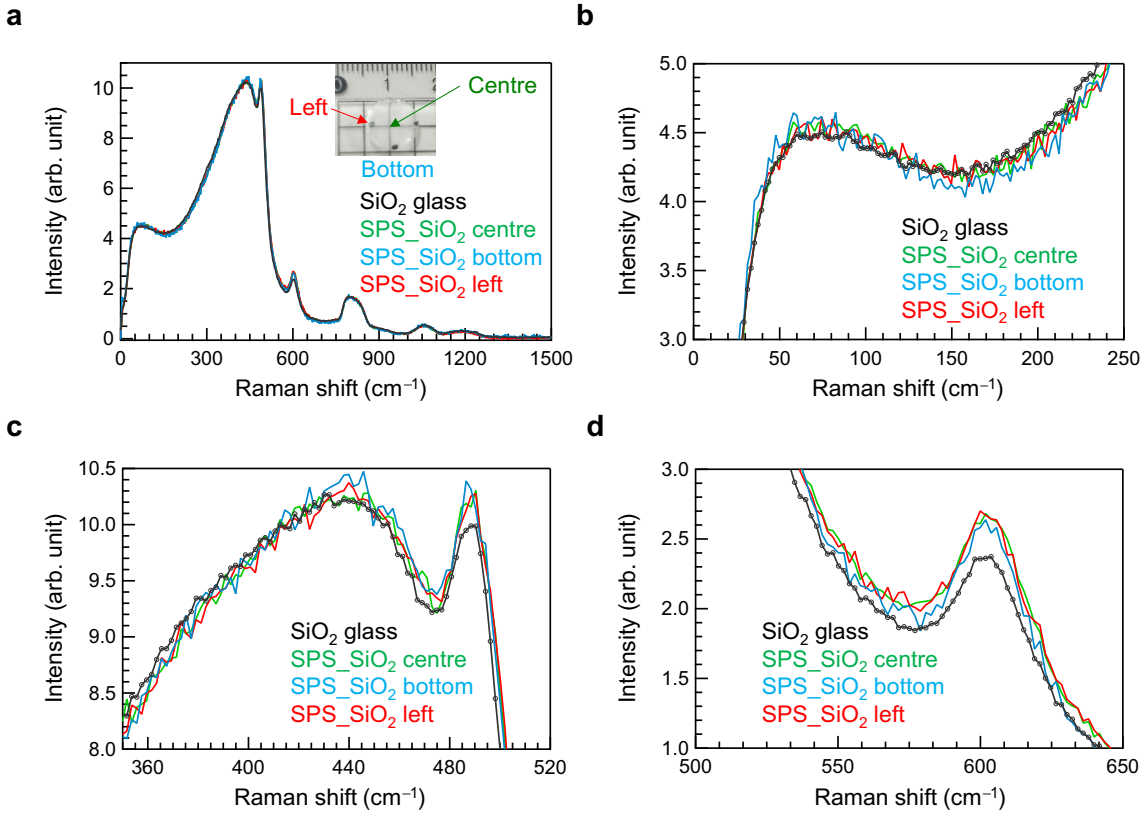

Figure 7. Micro-Raman spectra of SPS-SiO_2 glass recorded with HH polarisation. (**a**) Micro-Raman spectra of SPS-SiO_2 glass prepared at 6 MPa, 1400 °C along with that of SiO_2 glass. The inset shows the photograph of the SPS-SiO_2 glass marked with the measurement positions. Enlarged Raman spectra showing the (**b**) boson peak, (**c**) D_1 peak, and (**d**) D_2 peak.

samples are not in contact with any container, the interface between the materials and surrounding atmosphere is considered important. We believe that the influence of the interface on the structure and physical properties should be considered not only in SPS but also other manufacturing methods. Thus, ceramics with core–shell-like structures can be spontaneously prepared by selecting the fabrication method. In addition, we emphasise that different probes are required for different scales of constituents in a solid-state matrix. For example, because the relationship between elastic (macroscopic) properties and spectroscopic (microscopic) approaches is not straightforward, a combination of analytical methods is necessary for complete characterisation[45–47]. A deeper understanding of the structure of the materials is required for more precise control of the properties.

Conclusion

Transparent SPS-SiO_2 glasses without grain boundary or precipitation of crystallites were successfully prepared. The results of HEXRD, micro-IR spectroscopy, and micro-Raman spectroscopy suggest the formation of irregular silica species in the SPS-SiO_2 glass near the interface with the mould. Since the highest density of SPS-SiO_2 glass was attained prepared at lower pressure and higher temperature, it is expected that that the densification of SiO_2 glass is mainly due to reduction reactions, rather than conventional densification by applying GPa pressure. Although sintering can produce novel solid-state matrices, spatial analysis and macroscopic properties are important for understanding the nature of the sample.

Methods

Preparation. SiO_2 glasses were prepared by SPS of silica powder with a diameter of approximately 25 μm (99.999% purity; High Purity Chemicals). The SiO_2 powder was loaded into a graphite die with an inner diameter of 10 mm and sealed with two graphite punches. The sintering temperature was controlled according to the following sequence: the temperature was increased to 600 °C from approximately 25 °C in approximately 5 min, maintained at 600 °C for approximately another 5 min, increased again to 1300 or 1400 °C at a constant rate of 10 °C/min and then maintained for 15 min. The entire sintering process was carried out in vacuum, and a pressure of 6 or 70 MPa was applied between both ends of the graphite punch. After sintering, the sample was cooled without controlling the temperature. Four different preparation conditions were used in this study: 6 MPa, 1300 °C; 6 MPa, 1400 °C; 70 MPa, 1300 °C; and 70 MPa, 1400 °C. The obtained SiO_2 glass was surface polished and characterised using different methods.

Characterisation. A high-energy X-ray diffraction (XRD) experiment was performed using a two-axis diffractometer dedicated to the study of disordered materials at the BL04B2 beamline of the SPring-8 synchrotron radiation facility (Hyogo Japan)[48]. The energy of the incident X-rays is 61.43 keV. The raw data were corrected for polarisation, absorption, and background, and the contribution of Compton scattering was subtracted using a standard data analysis software.

The morphology of the samples was measured using a scanning electron microscope (SEM), where SEM images were taken using a JSM-6510(JEOL). An HF-2000 (Hitachi) microscope was used to obtain transmission electron microscopy (TEM) images. Transmittance measurements were performed at 25 °C using a spectrophotometer (UH-4150; Hitachi, Ltd.). The ultrasonic velocities of the longitudinal (V_L) and transverse (V_T) waves were measured at room temperature using the ultrasonic pulse-echo method (DPR300, JSR Ultrasonics). The frequencies of the longitudinal and transverse transducers are 10 and 5 MHz, respectively. The Young's modulus (E_0), instantaneous shear modulus (G_0), bulk modulus (K_0), and Poisson's ratio (v) were calculated according to previously reported methods[47]. The errors in E_0, G_0, and K_0 were less than ± 0.1 GPa.

The micro-Raman spectroscopy was performed in backscattering geometry using a single-frequency diode-pumped solid-state laser operating at 532 nm (Oxxius LCX-532S-300) and a custom-built microscope with ultra-narrowband notch filters (OptiGrate). The incident laser was attenuated to 7 mW and focused using a 50 × objective lens. The scattered light, collected by the same lens, was analysed using a single monochromator (Jovin-Yvon, HR320, 1200 grooves/mm) equipped with a charge-coupled device camera (Andor, DU420). The measurement system for Raman spectra is shown in a previous study[49]. We employed a multivariate analysis software Unscrambler 11 (Camo Analytics), which provides EMSC, to remove fluorescence-like broad baselines for the SPS samples.

Positron annihilation lifetimes were measured using a PSA TypeL-II system (Toyo Seiko Co., Ltd.) with an anti-coincidence system[50]. The ^{22}Na source, with a diameter of 15 mm, was encapsulated in a Kapton film. The accumulated count for each sample was 10^7.

Infrared spectra (in the mid-infrared (IR) region from 600 to 8000 cm^{-1}) were measured using the IR beamline BL43IR at the SPring-8 synchrotron facility (Hyogo, Japan). A Fourier transfer infrared (FTIR) microspectrophotometer (BRUKER model HYPERION IR microscope with a VERTEX70 FTIR spectrometer) was used with IR synchrotron radiation. The microscope has a motorised xy-stage, which is used to specify the measurement position. The magnification of the objective mirrors is 36 ×. The spatial resolution is approximately 20 μm at 2000–3000 cm^{-1}. The wavenumber resolution is 1 cm^{-1}, and the number of accumulations is 4000 times. The sample was set on a stainless steel mesh with a honeycomb array with a hole diameter of 2 mm. All the measurements were performed at room temperature. The infrared optical path was purged with dry air to remove water and CO_2 molecules (FT-IR purge gas generator; Parker Co., Ltd.).

Data availability

The authors declare that all relevant data supporting the findings of this study are available from the corresponding authors on request.

Received: 26 May 2022; Accepted: 22 August 2022
Published online: 30 August 2022

References

1. Tokita, M. Trends in advanced SPS spark plasma sintering systems and technology—Functionally gradient materials and unique synthetic processing methods from next generation of powder technology. *J. Soc. Powder. Tech. Jpn.* **30**, 790–804 (1993) (**in Japanese**).
2. Munir, Z. A., Anselmi-Tamburini, & Ohyanagi, U. M. The effect of electric field and pressure on the synthesis and consolidation of materials: A review of the spark plasma sintering method. *J. Mater. Sci.* **41**, 763–777 (2006).
3. Kondoh, I., Tanaka, T. & Tamari, N. Usefulness of spark plasma sintering on densification and mechanical properties of alumina whisker/zirconia composites. *J. Ceram. Soc. Jpn.* **102**, 505–507 (1994) (**in Japanese**).
4. Omori, M. Sintering, consolidation, reaction and crystal growth by the spark plasma system (SPS). *Mater. Sci. Eng. A.* **287**, 183–188 (2000).
5. Andrade, M. J. *et al.* Electrical conductive double-walled carbon nanotubes – Silica glass nanocomposites prepared by the sol–gel process and spark plasma sintering. *Scr. Mater.* **61**, 988–991 (2009).
6. Zhang, J., Tu, R. & Goto, T. Fabrication of transparent SiO_2 glass by pressureless sintering and spark plasma sintering. *Ceram. Int.* **38**, 2673–2678 (2012).
7. He, Z., Katsui, H. & Goto, T. Mechanical properties of nano-grain SiO_2 glass prepared by spark plasma sintering. *J. Euro. Ceram. Soc.* **37**, 721–725 (2017).
8. Okada, G., Kasap, S. & Yanagida, T. Radioluminescence and thermally-stimulated luminescence of SiO_2 glasses prepared by spark plasma sintering. *J. Ceram. Soc. Jpn.* **124**, 541–545 (2016).
9. Okada, G., Kasap, S. & Yanagida, T. Optically- and thermally-stimulated luminescences of Ce-doped SiO_2 glasses prepared by spark plasma sintering. *Opt. Mater.* **61**, 15–20 (2016).
10. Shiratori, D. *et al.* Dosimetric properties of Sn-doped SiO_2 glasses synthesized by the spark plasma sintering method. *Rad. Meas.* **134**, 106297 (2020).
11. Pacchioni, G., Skuja, L. & Griscom, D. L. *Defects in SiO_2 and Related Dielectrics: Science and Technology* (Kluwer Academic Publishers, 2000).
12. Skuja, L., Hirano, M., Hosono, H. & Kajihara, K. Defects in oxide glasses. *Phys. Stat. Sol. C.* **2**, 15–24 (2005).
13. Griscom, D. L. Trapped-electron centers in pure and doped glassy silica: a review and synthesis. *J. Non-Cryst. Solids.* **357**, 1945–1962 (2011).
14. Parc, R. L., Levelut, C., Pelous, J., Martinez, V. & Champagnon, B. Influence of fictive temperature and composition of silica glass on anomalous elastic behaviour. *J. Phys. Condens. Matter* **21**, 079802 (2009).
15. Kakiuchida, H., Sekiya, E. H., Shimodaira, N., Saito, K. & Ikushima, A. J. Refractive index and density changes in silica glass by halogen doping. *J. Non-Cryst. Solids* **353**, 568–572 (2007).

16. Masai, H. *et al.* Relationship between the first sharp diffraction peak and physical properties of silicon dioxide (SiO_2) glasses possessing different fictive temperatures. *J. Ceram. Soc. Jpn.* **128**, 1038–1044 (2020).
17. West, R. N. Positron studies of condensed matter. *Adv. Phys.* **22**, 263–383 (1973).
18. Brückner, R. Properties and structure of vitreous silica. *J. Non-Cryst. Solids* **5**, 123–175 (1970).
19. Ono, M., Hara, K., Fujinami, M. & Ito, S. Void structure in silica glass with different fictive temperatures observed with positron annihilation lifetime spectroscopy. *Appl. Phys. Lett.* **101**, 164103 (2012).
20. Zanatta, M. *et al.* Structural evolution and medium range order in permanently densified vitreous SiO_2. *Phys. Rev. Lett.* **112**, 045501 (2014).
21. Onodera, Y. *et al.* Structure and properties of densified silica glass: characterizing the order within disorder. *NPG Asia Mater* **12**, 85 (2020).
22. Salmon, P. S., Martin, R. A., Mason, P. E. & Cuello, G. J. Topological versus chemical ordering in network glasses at intermediate and extended length scales. *Nature* **435**, 75–78 (2005).
23. Price, D. L., Moss, S. C., Reijers, R., Saboungi, M. L. & Susman, S. Intermediate-range order in glasses and liquids. *J. Phys. C: Solid State Phys.* **21**, L1069–L1072 (1988).
24. Price, D. L. *et al.* The structure of phosphorus-selenium glasses I. Concentration dependence of the short- and intermediate-range order. *J. Non-Cryst. Solids* **66**, 443–465 (1984).
25. Murakami, M. *et al.* Ultrahigh-pressure form of SiO_2 glass with dense pyrite-type crystalline homology. *Phys. Rev. B* **99**(045153), 1–12 (2019).
26. Mauro, J. C., Gupta, P. K. & Loucks, R. J. Composition dependence of glass transition temperature and fragility. II. A topological model of alkali borate liquids. *J. Chem. Phys.* **130**, 234503 (2009).
27. Agarwal, A. & Tomozawa, M. Correlation of silica glass properties with the infrared spectra. *J. Non-Cryst. Solids* **209**, 166–174 (1997).
28. Fraser, D. B. Factors influencing the acoustic properties of vitreous silica. *J. Appl. Phys.* **39**, 5868 (1968).
29. Kakiuchida, H., Saito, K. & Ikushima, A. J. Precise determination of fictive temperature of silica glass by infrared absorption spectrum. *J. Appl. Phys.* **93**, 777–779 (2003).
30. Watanabe, T., Saito, K. & Ikushima, A. J. Fictive temperature dependence of density fluctuation in SiO_2 glass. *J. Appl. Phys.* **94**, 4824 (2003).
31. Xu, J. L. & Khor, K. A. Chemical analysis of silica doped hydroxyapatite biomaterials consolidated by a spark plasma sintering method. *J. Inorg. Biochem.* **101**, 187–195 (2007).
32. Gerber, T. & Himmel, B. The structure of silica glass in dependence on the fictive temperature. *J. Non-Cryst. Solids* **92**, 407–417 (1987).
33. Mantisi, B. *et al.* Non-Debye normalization of the glass vibrational density of states in mildly densified silicate glasses. *J. Phys. Condens. Matter.* **22**, 025402 (2010).
34. Malinovsky, V. K., Novikov, V. N. & Sokolov, A. P. Log-normal spectrum of low-energy vibrational excitations in glasses. *Phys. Lett. A* **153**, 63–66 (1991).
35. Hubbard, B. E., Tu, J. J., Agladze, N. I. & Sievers, A. J. Optical activity of the boson peak and two-level systems in silica-germania glasses. *Phys. Rev. B* **67**, 144201 (2003).
36. Inamura, Y. *et al.* Intermediate range structure and low-energy dynamics of densified vitreous silica. *J. Non-Cryst. Solids* **293–295**, 389–393 (2001).
37. Pasquarello, A. & Car, R. Identification of Raman defect lines as signatures of ring structures in vitreous silica. *Phys. Rev. Lett.* **80**, 5145–5147 (1998).
38. McMillan, P. F., Wolf, G. H. & Poe, B. T. Vibrational spectroscopy of silicate liquids and glasses. *Chem. Geol.* **96**, 351–366 (1992).
39. Barrio, R. A., Galeener, F. L., Martínez, E. & Elliott, R. J. Regular ring dynamics in AX_2 tetrahedral glasses. *Phys. Rev. B* **48**, 15672 (1993).
40. Kantelhardt, J. W., Russ, S. & Bunde, A. Excess modes in the vibrational spectrum of disordered systems and the boson peak. *Phys. Rev. B* **63**, 064302 (2001).
41. Skogholt, J., Liland, K. H. & Indahl, U. G. Preprocessing of spectral data in the extended multiplicative signal correction framework using multiple reference spectra. *J. Raman Spectrosc.* **50**, 407–417 (2019).
42. Skinner, L. B. *et al.* A time resolved high energy X-ray diffraction study of cooling liquid SiO_2. *Phys. Chem. Chem. Phys.* **15**, 8566–8572 (2013).
43. Champagnon, B., Wondraczek, L. & Deschamps, T. Boson peak, structural inhomogeneity, light scattering and transparency of silicate glasses. *J. Non-Cryst. Solids* **355**, 712–714 (2009).
44. Deschamps, T. *et al.* Silica under hydrostatic pressure: A non continuous medium behavior. *J. Non-Cryst. Solids* **355**, 2422–2424 (2009).
45. Masai, H. *et al.* Correlation between structures and physical properties of binary $ZnO–P_2O_5$ glasses. *Phys. Status Solidi B* **257**, 2000186 (2020).
46. Masai, H. *et al.* Examination of structure and optical properties of Ce^{3+}-doped strontium borate glass by regression analysis. *Sci. Rep.* **11**, 3811 (2021).
47. Masai, H., Fujii, Y., Kitamura, N. & Yamawaki, M. Relationship between the elastic properties and structure of BaO-TiO_2-GeO_2-SiO_2 glasses. *J. Non-Cryst. Solids* **576**, 121248 (2022).
48. Kohara, S. *et al.* Structural studies of disordered materials using high-energy x-ray diffraction from ambient to extreme conditions. *J. Phys. Condens. Matter* **19**, 506101 (2007).
49. Fujii, Y., Katayama, D. & Koreeda, A. Broadband light scattering spectroscopy utilizing an ultra-narrowband holographic notch filter. *Jpn. J. Appl. Phys.* **55**, 10TC03 (2016).
50. Yamawaki, M., Kobayashi, Y., Hattori, K. & Watanabe, Y. Novel system for potential nondestructive material inspection using positron annihilation lifetime spectroscopy. *Jpn. J. Appl. Phys.* **50**, 086301 (2011).

Acknowledgements

This work was partially supported by the Japan Society for the Promotion of Science Grant-in-Aid for Scientific Research (B) Numbers JP18H01714, JP22H01785 (H.M.), (C) JP19K05252 (Y.F.), for Challenging Research (Exploratory) Number 19K22072 (H.M. and S.K.), and for Transformative Research Areas (A) "Hyper-Ordered Structures Science" Grant Numbers 20H05878 and 20H05881 (S.K.), 20H05880 (A.M.), and 20H05882 (H.M.). High-energy XRD was performed using the BL04B2 beamline at SPring-8, with the approval of the Japan Synchrotron Radiation Research Institute (JASRI) (Proposal Nos. 2020A1494 and 2021A1166). Micro-IR measurements were performed using the BL43IR beamline at SPring-8 with the approval of the JASRI (Proposal Nos. 2021A1144 and 2021B1149). The author (H.M.) is grateful for discussions with Dr. M. Yamawaki.

Author contributions

H. M. formulated the research project. H. K. and T. Y. performed the materials preparation. N. K. measured the elastic modulus. H. M. performed optical absorption, positron decay measurement. A. M. measured density of the samples. T. M. performed SEM and TEM observation. S. K. and H. M. performed XRD measurements and analysed the resulting data. H. M. and Y. I. performed micro-IR measurement. Y. F. performed micro-Raman measurement. H. M. wrote the paper. All authors discussed the results and commented on the manuscript.

Competing interests

The authors declare no competing interests.

Additional information

Supplementary Information The online version contains supplementary material available at https://doi.org/10.1038/s41598-022-18892-4.

Correspondence and requests for materials should be addressed to H.M.

Reprints and permissions information is available at www.nature.com/reprints.

Publisher's note Springer Nature remains neutral with regard to jurisdictional claims in published maps and institutional affiliations.